

Dynamics and structure in complex liquids under shear explored by neutron scattering

Max Wolff* and Andreas Magerl

Lehrstuhl fuer Kristallographie und Strukturphysik, Universitaet Erlangen-Nuernberg, 91054 Erlangen, Germany

Bernhard Frick

Institute Laue-Langevin, 38042 Grenoble, France

Hartmut Zabel

Lehrstuhl fuer Experimentalphysik/Festkoerperphysik, Ruhr-Universitaet Bochum, 44780 Bochum, Germany

(Received 21 August 2004; published 24 January 2005)

It is well established that the structural order of macromolecules can be affected by the application of shear. For example, triblock copolymers in aqueous solutions are known to aggregate for high concentrations. For increasing temperature the polymer micelles crystallize and offer a model system for the investigation of percolation and crystallization. The crystalline phases rearrange under shear. We correlate the structural assemblages of polymer micelles to the microscopic dynamics of the polymer monomers as well as to the solvent molecules at rest and under shear. We find the monomer dynamics affected by the different arrangements of the polymer micelles in aqueous solutions. For pronounced structural ordering we report on the monomer diffusion to become anisotropic under shear, with the diffusive mode in the direction of the shear gradient being slowed down with respect to that in the direction of the flow.

DOI: 10.1103/PhysRevE.71.011509

PACS number(s): 61.12.Ex, 83.60.Rs, 83.80.Uv

I. INTRODUCTION

Since the pioneering experiments by Keller *et al.* published in 1970 [1], it has been well known that polymer solutions may crystallize under certain conditions. Throughout the 1980s a more detailed picture of a microscopic scale of crystallization was obtained by the use of small-angle neutron scattering (SANS) [2–5]. Diat and co-workers investigated the shear dependence of structural ordering systematically by light and neutron scattering. In analogy to a phase diagram without shear applied they presented different orientational states of the sample induced by shear. These were summarized in a phase diagram as a function of composition and shear rate [6–8].

Applied shear breaks the isotropy of the sample. The key parameter to measure shear macroscopically (on the mm length scale) is the mean shear gradient calculated from the sample velocity and the geometry of the shear device. To describe the anisotropy induced on the molecular scale, in addition, a local shear gradient has to be defined as a microscopic (on the nm length scale) velocity gradient. The two values calculated from these definitions may differ and it is well established that depending on the properties of the solid-liquid interface surface slip [9–12] or, in the case of inhomogeneities in the sample during the reorientation process, shear banding may occur [13–18]. To gain information on the macroscopic velocity profile of liquids, different techniques such as NMR, supersonic [19], light scattering

[20,21], and neutron scattering [22] have been employed.

Aside from the effect that shear has on structural arrangements, it has also been noticed from theoretical considerations that shear may affect the microscopic diffusion [23–26]. On a molecular scale, nonequilibrium molecular dynamic (NEMD) simulations have shown an anisotropy of the self-diffusion tensor under shear [27–31]. For colloidal systems this has been demonstrated experimentally [32–34] and in simulations [35]. For the anisotropy of self-diffusion under shear different mechanisms have to be considered: (i) Anisotropic particles may orient in shear fields. (ii) Anisotropy is induced in the local environment of the particles.

To date there is no experimental proof of an influence of shear on the dynamics of molecules on the nm length scale. In the present work we elucidate by different neutron scattering techniques that the local dynamics of polymer molecules are correlated to the dynamics and structure of polymer micelles. This results in an effect of shear on the local modes even if the Peclet number (see Sec. II for the definition) for the single-polymer monomer is too small to expect a direct influence of shear, whereas it is big enough for the micelle. As an additional parameter we varied the degree of structural ordering in the sample by using solid interfaces with different chemical terminations. With investigations along the presented line a deeper understanding of the correlation of the local dynamics to the structural arrangements and in particular to the influence of shear becomes possible.

II. NEUTRON SCATTERING AND DIFFUSION

We have used several neutron scattering techniques to obtain information on the structure as well as on the dynamics of complex liquids.

*Permanent address: Institute Laue-Langevin, 38042 Grenoble, France. Present address: Lehrstuhl fuer Experimentalphysik/Festkoerperphysik, Ruhr-Universitaet Bochum, 44780 Bochum, Germany. Electronic address: v-wolff@ill.fr

A. Neutron scattering

The quantity measured in a scattering experiment is the scattered intensity with respect to different scattering angles and energy transfers. Two different scattering functions can be defined for neutron scattering experiments [36]:

$$S_{coh}(\mathbf{Q}, \omega) = \int K(\mathbf{r}, t) e^{i(\mathbf{Q}\cdot\mathbf{r} - \omega t)} d\mathbf{r} dt, \quad (1)$$

$$S_{inc}(\mathbf{Q}, \omega) = \int K_s(\mathbf{r}, t) e^{i(\mathbf{Q}\cdot\mathbf{r} - \omega t)} d\mathbf{r} dt. \quad (2)$$

The coherent structure factor $S_{coh}(\mathbf{Q}, \omega)$ represents the mean value of the scattering length density distribution in the sample. It is the Fourier transform in time and space of the inter-particle-correlation and particle self-correlation functions. $S_{coh}(\mathbf{Q}, \omega)$ gives information about the spatial order of the atoms in the sample and their evolution in time, and it describes the Bragg reflections, liquid structure factor, and phonon scattering. The incoherent structure factor $S_{inc}(\mathbf{Q}, \omega)$ is the Fourier transform in time and space of the particle self-correlation function and represents the deviation from the mean scattering length density in the sample. Accordingly, $S_{inc}(\mathbf{Q}, \omega)$ provides information on the self-diffusion of a specific particle.

For a random jump diffusion a Gaussian distribution of the so-called intermediate scattering function $I(\mathbf{Q}, t)$, which is the Fourier transform of $K_s(\mathbf{r}, t)$ [Eq. (2)] with respect to r , can be assumed [37],

$$I(\mathbf{Q}, t) = e^{-DtQ^2}, \quad (3)$$

which gives the following scattering function:

$$S(\mathbf{Q}, \omega) = \frac{1}{\pi} \frac{DQ^2}{\omega^2 + (DQ^2)^2}. \quad (4)$$

This is a Lorentz distribution with the full width at half maximum (HWHM) Γ :

$$\Gamma = DQ^2. \quad (5)$$

B. Diffusion in liquids

Following the Stokes-Einstein-Debye model, the translational diffusivity D_{trans} of a particle in a liquid can be related to the viscosity η [38,39]:

$$D_{trans} = \frac{k_B T}{6\pi\eta R}, \quad (6)$$

with k_B the Boltzmann constant, T the temperature, and R the particle radius. For a more detailed picture one has to distinguish between different types of diffusion. For an isolated particle, moving in a potential free environment, the Stokes-Einstein-Debye limit holds. The time scale of relevance is given by $\tau_B = m/6\pi\eta R$, where m denotes the mass of the particle. This is the time frame for velocity fluctuations. Within this time a particle moves only a small part of its radius. For an ensemble of particles the interparticle interac-

TABLE I. Coherent and incoherent scattering powers of the different components of the sample.

	Coherent	Incoherent
P85	5.0%	74.4%
D ₂ O	16.3%	4.3%

tion potential has to be considered in addition. The dominant time scale becomes then $\tau_I = a^2/D_{trans}$, during which the particle travels a distance such that it is affected by differences in the surrounding potential. The parameter $a = 2R\Phi^{-1/3}$ denotes an effective particle radius, and Φ is the volume fraction of particles in the solution. The relevant length scale a is obtained from the maximum of the structure factor.

For judging the relative importance of shear as compared to the thermal mobility of the particles one can define the Peclet number:

$$Pe = \dot{\gamma}\tau_I, \quad (7)$$

where $\dot{\gamma}$ denotes the shear rate. For small Peclet numbers ($Pe \ll 1$) the diffusive process is completely dominated by thermal motion. For high Peclet numbers ($Pe \gg 1$) the particle motion is strongly affected by the shear field as the surrounding of a certain particle is changing on the time scale τ_I .

III. EXPERIMENTAL DETAILS

A. Sample

Our sample consists of a 33% solution (in weight) of the triblock copolymer P85 (EO₂₅PO₄₀EO₂₅) in deuterated water. The P85 was obtained from BASF Wyandotte Corp. (Mount Olive, NJ) and was used without further purification. P85 has a molecular mass of about 4500 u and the hydrophobic part of the molecule is 50%. The coherent and incoherent scattering powers, with respect to the total scattering power, of the different components of the sample are summarized in Table I. The dominant contribution is the incoherent scattering from the hydrogen in the polymer molecules. The coherent scattering from the deuterated water is about one-sixth of the total scattering. The scattering length density SLD of the deuterated water is $SLD = 6.5 \times 10^{-6} \text{ \AA}^{-2}$ and that of the polymer $SLD = 0.44 \times 10^{-6} \text{ \AA}^{-2}$. This gives a good contrast between the two components for spectroscopic as well as for diffraction studies.

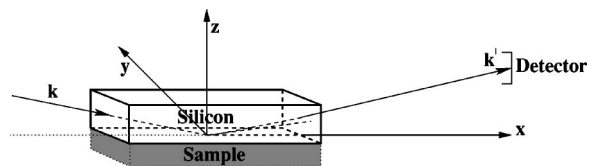


FIG. 1. Scattering geometry for the reflectivity studies. After scattering at the solid-liquid interface the neutrons are detected by a position-sensitive detector.

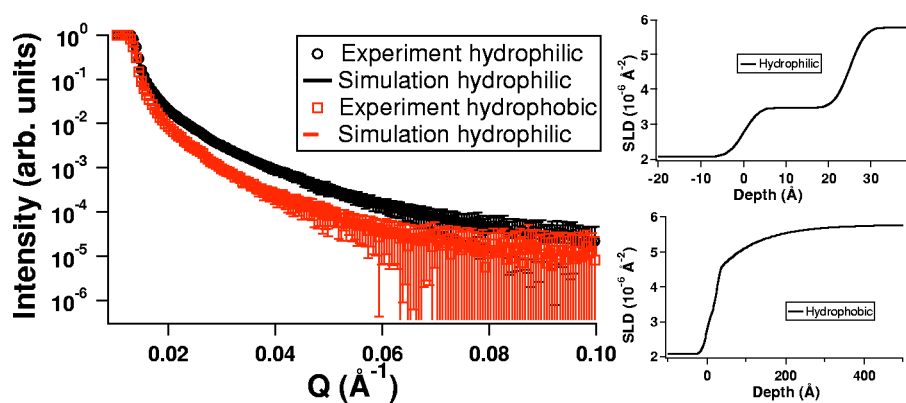


FIG. 2. Specular-reflected intensity for water at a hydrophilic and a hydrophobic-coated silicon interface (left panel). In the right panels the scattering length density SLD profiles for the silicon-water interface are shown, which have been used for the simulation of the data (solid lines in the left panel).

The phase diagram with respect to polymer concentration and temperature has been established by SANS [40]. Different phases from unimer over micelles to cubic and lamellar structures have been reported. For low concentrations and temperatures the polymer monomers are solved in the water. With increasing temperature or concentration they start to agglomerate into micelles and as the critical micelle volume fraction is reached they crystallize. The concentrated gel-like phases may form a single-crystalline state under shear [41–43]. Using contrast variation techniques in SANS measurements, the internal structure of the micelles has been determined [44]. The core and shell of the micelles contain about 50% and 90% of water, respectively. For a theoretical approach the interaction potential between the micelles can be treated according to the core and gown model [45–48]. The translational diffusion coefficient of similar polymer monomers in aqueous solutions as determined by light scattering is on the order of $10^{-7} \text{ cm}^2 \text{ s}^{-1}$ and it was found nearly independent of temperature and concentration [49]. These polymer solutions are expected to behave similar to P85 for which no diffusion constants are available.

The P85-water solutions were prepared at a temperature of 278 K, where the polymer is solvable in water. During and after filling the sample cell was kept at the same temperature to prevent shear-induced ordering prior to the measurement.

B. Solid interface

Two single-crystalline polished silicon wafers have been prepared as solid interfaces. One surface was oxidized through treatment in Carroic acid (5:1 mixture of H_2SO_4 and H_2O_2) for 15 min. It is known that SiO_2 forms at the surface, which gives it a hydrophilic character. The second silicon wafer was dipped for one minute in HF. The surface coverage with hydrogen provides the desired hydrophobic character for at least the time needed for the measurement.

To confirm the properties of the two silicon wafers we performed reflectivity studies of pure deuterated water with the instrument ADAM at the Institute Laue-Langevin (ILL, Grenoble, France) [50]. For a more detailed description we refer to Sec. III D 2. ADAM is an angle-dispersive reflectometer using a fixed wavelength of 4.41 \AA . The scattering geometry is shown in Fig. 1. Neutrons from the monochromator travel through a silicon wafer and are scattered at the

silicon-liquid interface. The path length of the neutrons through the silicon wafer is about 120 mm which results in a reduction of the intensity by absorption of about 20%.

Figure 2 shows the specular (incident equals exit angle) reflected intensity of the hydrophilic and hydrophobic interface (left panel) in contact with deuterated water. A correction for the incident beam footprint has been applied. First the two silicon wafers were measured against air. The scattering length density profiles obtained were used as fixed parameters for the later measurements. The right panels in Fig. 2 show the scattering length density profiles obtained. For the hydrophilic interface a three-region box model with bulk silicon, a silicon oxide layer of 25 \AA thickness, and bulk water with a roughness of 4 \AA at the interfaces fits the data well. The scattering length density of the D_2O ($\text{SLD} = 6 \times 10^{-6} \text{ \AA}^{-2}$) is slightly reduced due to impurities of about 10% of light water ($\text{SLD} = -0.5 \times 10^{-6} \text{ \AA}^{-2}$). However, for water in contact with the hydrophobic interface, the specular-reflected intensity drops off much faster, indicative of an increased roughness at the interface. The fit confirms that for the hydrophobic interface the data cannot be fitted by a three-box model. A reduced density of the water within a thickness of 20 nm has to be assumed at the interface.

Two different explanations for this depleted region of reduced density have been proposed. Either the density of the bulk water is reduced close to the hydrophobic interface due to structural defects or air nanobubbles may exist close to the interface. A region of reduced density has been calculated from theoretical considerations [51,52]. However, the predicted thickness of 2 nm is much smaller than found in our experiment. With the technique of atomic force microscopy (AFM) the existence of a 30-nm-thick layer of air bubbles in water has been demonstrated close to a hydrophobic interface [53]. In a more recent and detailed neutron reflectivity study it has been shown that air bubbles may be induced by the AFM cantilever and that a thinner layer is found in the undisturbed sample [54,55]. However, the mentioned experiments were in variance to ours performed with degassed water. The scattering length density profile fitted to the present measurement and the thick depleted layer we found close to the hydrophobic interface cannot be explained by structural depletion. As we used water without degassing it the reduced scattering density found in the interface region in our measurements is most likely to be explained by the presence of air bubbles.

C. Shear devices

We have developed several shear devices for the investigation of liquids under shear with different neutron scattering techniques. Two possibilities can be envisaged: either a flow cell where liquid is pressed through a slit by the application of pressure or a shear cell where the liquid is confined between a fixed and a moving surface. The main difference is that for the flow cell the velocity profile will be parabolic whereas for the shear cell one expects a linear velocity profile.

For non-Newtonian and for highly viscous liquids flow cells have two major disadvantages. First, high pressures are needed to achieve high shear rates. This pressure may change the structural [56] as well as the dynamical properties [57] of the sample. In addition a pressure gradient will develop in the longitudinal direction throughout the slit leading to a superposition of the sample properties for different pressures, which are difficult to interpret. Second, the parabolic velocity profile implies that the shear gradient is not constant throughout the scattering volume. A liquid showing shear thinning will become thinned in regions with a high shear gradient—i.e., close to the walls. In the middle of the slit where the shear gradient is low, it will be thickened. This leads, as scattering contributions from all over the slit are registered, to an averaging over regions with different shear gradients. Because of these considerations, we decided to use shear cells for the experiments reported here. Couette-type devices have a curved interface and are not suited for scattering from the solid-liquid interface. In addition, it is difficult to probe a certain direction of the flow in spectroscopic measurements as the neutron beam traverses a Couette cell twice.

For the present diffraction study we used a plate-plate shear device equipped with different silicon wafers which had a diameter and a thickness of 200 mm and 11 mm, respectively. Figure 1 shows schematically the scattering geometry for reflectivity measurements. For the shear device the lower surface (not shown in the sketch) moves in the x direction and the momentum transfer is always parallel to the shear gradient. To minimize the gradient in the velocity of the rotating disk and the shear gradient and to use a large interface the neutron beam passes the cell tangential at a radius of 70–90 mm. A rotating aluminum plate is positioned at an adjustable distance of about 1 mm from the silicon disk.

The shear device used for the spectroscopic studies was also equipped with different silicon wafers with a thickness of 0.625 mm on the surface of the fixed and rotating disks. Special attention has been given not to cover the neutron window with any glue containing hydrogen. Figure 3 shows the scattering geometry for the neutron spectroscopy measurements. The presented data were taken at different scattering angles again with scattering from the outer part (70–90 mm) of the moving and static disks. In reflection geometry (left panel) the vector of momentum transfer Q is parallel to the shear gradient and in transmission geometry Q is parallel to the flow of the liquid. Thus it is possible to distinguish the influence of shear on the microscopic dynamics in these two directions. In addition, in transmission ge-

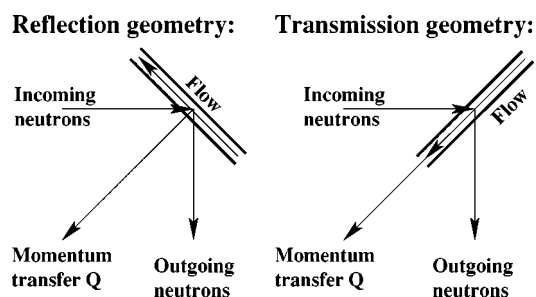


FIG. 3. Scattering geometry for neutron spectroscopy. The incoming and outgoing beam defines the scattering plane. The shear device is placed perpendicular to it. For the reflection geometry (left panel) Q is parallel to the shear gradient whereas for the transmission geometry (right panel) it is parallel to the macroscopic flow.

ometry the inelastic Doppler-scattered neutrons can provide information on the macroscopic flow. The shear devices used for the diffraction studies and for the spectroscopic measurements are described elsewhere in more detail [58].

D. Instruments

1. Rheologie

The rheological measurements have been made using a commercial rheometer (Paar Physica USD 200). The temperature was controlled by flowing water, which was heated and cooled by a HAAKE DC50 water bath. As the viscosity of the sample changes by several orders of magnitude for the different phases with a maximum viscosity of about 1000 Pas we used a cone-plate geometry with a cone diameter of 30 mm. A certain shear rate was applied to the sample and the torque necessary to turn the cone has been measured. The cone as well as the plate were made from stainless steel.

2. Reflectometry

The reflectivity studies were carried out on the instrument ADAM at the ILL. ADAM follows the principle of a two-circle diffractometer with a fixed wavelength of 4.41 Å. The data are collected by a two-dimensional position-sensitive detector covering an angular range of $\pm 3^\circ$. The scattering plane on this instrument is horizontal.

The x , y , and z directions (Fig. 1) are defined with respect to the surface of the sample, with z being the normal of the interface, x being in the plane of the interface and defined by the incident beam direction k , and y is in the plane of the interface and perpendicular to x . For a momentum transfer of $|Q|=0.04 \text{ \AA}^{-1}$ the resolution $\Delta Q_x=1 \times 10^{-5} \text{ \AA}^{-1}$ is determined by the pixel size of the detector and the scattering angle. The resolution $\Delta Q_z=7.5 \times 10^{-4} \text{ \AA}^{-1}$ is given by vertical slits. The resolution $\Delta Q_y=7.5 \times 10^{-2} \text{ \AA}^{-1}$ is given by the height of the focusing monochromator and the distance of the sample from the monochromator.

The resolution used allows investigations of lattice constants of up to 100 nm in the z direction and 5 μm in the x direction. The resolution in the y direction was relaxed and the small-angle scattering from structures larger than about 50 Å could not be resolved. For the present samples the

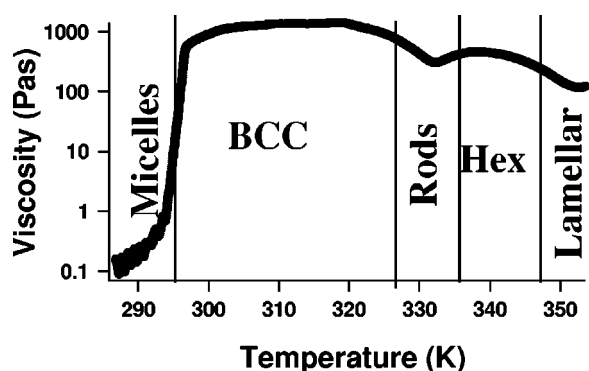


FIG. 4. Viscosity for a 33% (in weight) solution of P85 in water measured at a shear rate of $\dot{\gamma}=1 \text{ s}^{-1}$ as a function of temperatures.

polymer micelles have a diameter of about 60 Å. Therefore we had a strong contribution from small-angle scattering on the specular line due to the smearing out of the structure factor for low Q values. All reflectivity data have been corrected for the calculated footprint of the shear device and for the small-angle scattering by subtraction off the scattered intensity for an offset angle of $\Delta\alpha = \alpha - \alpha' = 0.2^\circ$ (α , incident angle; α' , exit angle) in the scattering plane from the specular signal $\alpha = \alpha'$.

The height of the beam at the sample position was 2 cm, resulting in a gradient of the shear rate and rotating disk velocity of about 20%.

3. Spectroscopy

Different spectrometers were used to cover a large range of relaxation times from the ns to the ps region.

The backscattering experiments with an energy resolution of about 1 μeV [full width at half maximum (FWHM)] have been made on the instrument IN16 (ILL). This instrument uses a wavelength of 6.271 Å. The multidetector registered the neutrons for the static measurements and one single helium tube for the measurements with the shear device. The backscattering data were fitted by one Lorentzian line without convolution of the narrow resolution function. To obtain information on the temperature dependence of the diffusion coefficients we measured the elastic scattered intensity that is directly correlated to the quasielastic linewidth.

The time-of-flight experiments with the unsheared sample have been carried out at the NEAT spectrometer at the HMI (Germany) with a wavelength of 5.1 Å, resulting in a resolution of 93 μeV (FWHM).

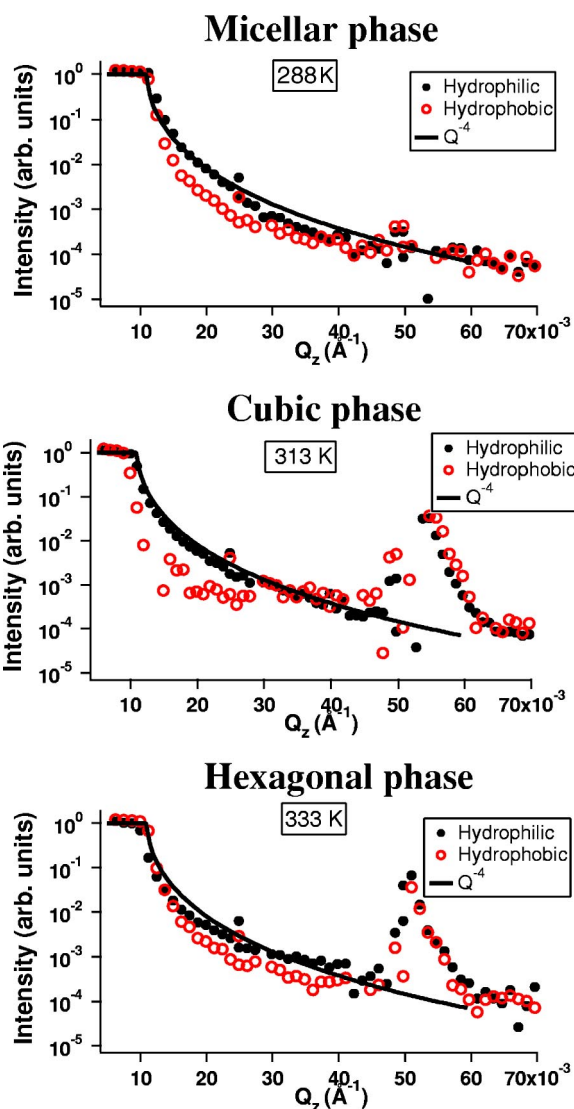


FIG. 5. Specular reflected intensity for a 33% (in weight) solution of P85 in deuterated water for 288 K (upper panel), 313 K (middle panel), and 333 K (lower panel) at hydrophilic and hydrophobic-coated solid interfaces. For all temperatures the intensities taken at the hydrophobic interface drop faster than for the hydrophilic one. For temperatures above 290 K, a Bragg reflection from the crystalline phase becomes visible at $Q_z \approx 0.055 \text{ \AA}^{-1}$.

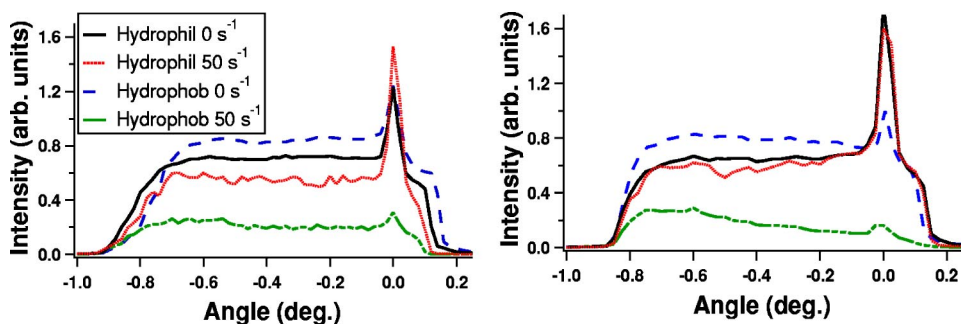


FIG. 6. Rocking curve of the first-order Bragg reflection for a temperature of 313 K (left panel) and 333 K (right panel).

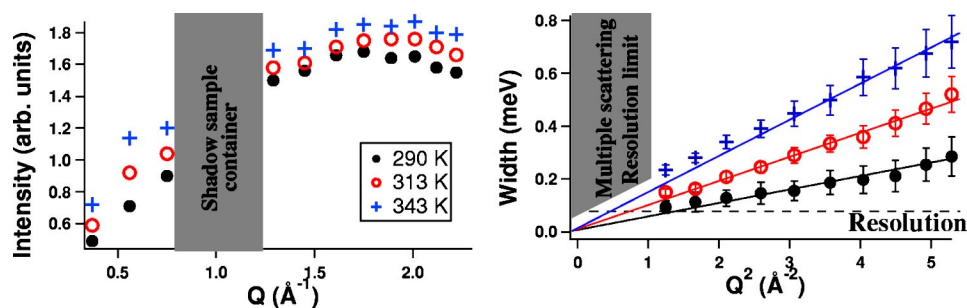


FIG. 7. Structure factor (left panel) and Q dependence of the linewidth for the broader quasi-elastic line at three different temperatures.

The triple-axis experiments were performed with IN3 (ILL) with a resolution of $160 \mu\text{eV}$ (FWHM).

The quasielastic spectra taken without the shear device were corrected for the detector efficiency and the empty sample container. Afterwards they were fitted by a convolution of two Lorentzian lines with the measured resolution function. The width of the more narrow Lorentzian line was fixed at the value determined from the backscattering data.

For the shear device a subtraction of the empty cell is rather difficult. Alternatively the elastic scattering from the cell was fitted separately and added to the quasielastic line fitted to the spectra shown in Fig. 12, below.

IV. RESULTS

A. Rheology

Figure 4 shows the result of a temperature sweep with the 33% (in weight) solution of P85 in water for an applied shear rate of 1 s^{-1} . The discontinuities in the viscosity can readily be correlated with the structural phase transitions found earlier in SANS studies [40]. For low temperatures the sample is in the micelle phase with weak correlations between the micelles. This results in a low viscosity of about 0.1 Pas. The scatter of the data points are caused by the instrumental setup, optimized for the high viscosity in the crystalline phase. At a temperature of 295 K the micelles organize in a cubic lattice and as consequence the viscosity increases by about four orders of magnitude. For the rod micelle phase the viscosity decrease is explained by weaker connections between the micelles and their anisotropic shape. For the more organized hexagonal and lamellar phases the viscosity is again high but because of the high temperature does not reach the value of the cubic phase. Thus the viscosity is directly correlated to the structural state of the sample.

In the micellar phase, there are no long-range correlations. From the viscosity of $\eta \approx 0.1 \text{ Pas}$ and a micellar radius of $R \approx 60 \text{ \AA}$ [44] the diffusion constant of the micelles can be calculated to $3.5 \times 10^{-9} \text{ cm}^2 \text{ s}^{-1}$ according to the Stokes-Einstein-Debye relation [Eq. (6)].

B. Reflectivity

To investigate the influence of different interfaces with different chemical terminations on the structural phases, we studied reflectivity profiles using the instrument ADAM (ILL). Figure 5 shows the specular-reflected intensity for a 33% solution of P85 in deuterated water, plotted as a function of Q_z . At 288 K (upper panel in Fig. 5) the sample is in

the liquid phase, whereas at 313 K (middle panel) and 333 K (lower panel) it is in the crystalline phase. All data have been corrected for the footprint and small-angle scattering. For Q_z values $> 0.02 \text{ \AA}^{-1}$, the intensity is dominated by small-angle scattering of the polymer micelles.

Nevertheless, the data clearly reveal a faster drop of the reflected intensity for the sample in contact with the hydrophobic surface than with the hydrophilic one. The steeper drop-off signals an increased surface roughness as already found for pure deuterated water. This can be explained in two ways. First, there might exist air bubbles close to the hydrophobic interface as found for the same interface in contact with water. Second, the polymer micelles with a hydrophilic shell try to avoid being close to the hydrophobic surface and may not be able to arrange themselves into a crystalline phase. Recently it has been shown that the adsorption and crystallization of Pluronic micelles is suppressed at a hydrophobic interface whereas it is favored close to a hydrophilic one, which supports the latter possibility [59].

The second feature revealed by the reflectivity data is the Bragg reflection at $Q_z \approx 0.055 \text{ \AA}^{-1}$ for temperatures above 290 K. This peak shifts towards smaller Q values for higher temperatures, which shows an increased layer sequence in good agreement with earlier SANS studies.

C. Diffraction

Figure 6 shows rocking scans along Q_x of the Bragg reflection at $Q_z \approx 0.055 \text{ \AA}^{-1}$ for the sample in the crystalline phase at 313 K (left panel) and 333 K (right panel). The intensity is plotted versus the offset angle $\Delta\alpha = \alpha - \alpha'$. $\Delta\alpha = 0$ defines the Bragg peak at the specular-reflected intensity. All data sets show a line shape with two components: a nearly equally distributed off-specular scattering and a narrow peak at the specular position. The narrow component reflects long-range orientational correlations as found, e.g., for epitaxial niobium on sapphire substrates [60]. It can be concluded that the lattice planes are on average flat over more than $10 \mu\text{m}$. The broader component is due to Bragg scattering from the mosaicity and size of the crystallites. A decision whether the broadening is caused by mosaicity or the crystallites size cannot be made only from the first-order reflection. The asymmetry of the diffuse scattering is a result of the accessible angular range for this particular measurement and contains no physical information. The broad component is wider than the accessible angular range, defined by the sample horizon, and indicates correlations on all length scales bigger than several μm .

At rest (shear rate $\dot{\gamma}=0$) we find that the broad component is more intense for the hydrophobic interface whereas the narrow one is more intense for the hydrophilic one. This means that the long-range orientational correlation of the polymer micelles is more pronounced at the hydrophilic interface, whereas close to the hydrophobic interface a structure with defects is formed. This is in good agreement with the conclusions drawn from the specular-reflected intensity.

For a shear rate of 50 s^{-1} the data sets taken at the different interfaces become more distinct. For the hydrophobic interface the intensity of the narrow as well as of the broad intensity component of the rocking curve becomes clearly decreased, showing a melting of the crystalline structure. For the hydrophilic interface both components are hardly affected by the shear. At 313 K the narrow component increases while the broad component decreases, indicating an enhanced ordering under shear. For both temperatures it turns out that the narrow component becomes predominant, implying more pronounced long-range orientational correlations for the hydrophilic interface. This clearly demonstrates that shear enhances the structural correlations close to a hydrophilic interface whereas it destroys the correlations close to a hydrophobic one.

D. Spectroscopy

To characterize the dynamic properties of the sample we need to distinguish between the mobility on different time scales. We separate between the motion of the water molecules, which act as solvent, and that of the polymer molecules.

1. Solvent

The dynamics of the sample in the ps range was investigated with the time-of-flight neutron spectrometer NEAT at the HMI (Germany) and the triple-axis spectrometer IN3 (ILL). Figure 7 shows the result of a measurement with a 0.6 mm (10% scattering) thick sample of the 33% solution of P85 in deuterated water. All data were fitted by two Lorentzian lines, convoluted with the measured instrumental resolution. The width of the narrow component was determined from the fit of the neutron backscattering data described in the next Sec. IV D 2. The left panel shows the structure factor of the wider component plotted against Q and the right panel shows the linewidth plotted as a function of Q^2 . The FWHM was determined with an error of 10%. The structure factor has a peak at 1.8 \AA^{-1} . From the literature it is known that the maximum of the structure factor for heavy water is

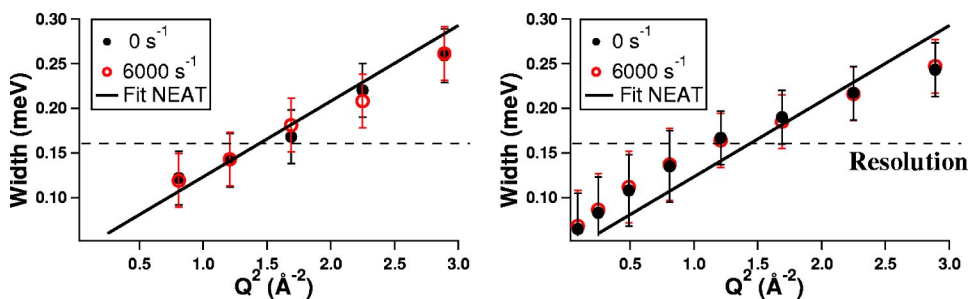


FIG. 8. Linewidth for the faster mode with the sample in reflection (left panel) and transmission (right panel) geometry at rest (solid circles) and for a shear rate of 6000 s^{-1} (open circles).

TABLE II. Diffusion constants found for the deuterated water for different temperatures.

T [K]	290	313	343
D [$10^{-6} \text{ cm}^2/\text{s}$]	4.03 ± 0.5	7.27 ± 0.4	10.7 ± 0.6

located at 2 \AA^{-1} [61,62]. Data points at about $Q=1 \text{ \AA}^{-1}$ are missing as a consequence of the shadow of the sample container in this direction.

The linewidth (right panel) shows a Q^2 dependence revealing a translational diffusion. By assuming a random jump diffusion from the slope of the linewidth the diffusion constant can be calculated [Eq. (5)]. The results for the three different temperatures are summarized in Table II. The diffusion constant at 313 K is found to be $7.27 \times 10^{-6} \text{ cm}^2 \text{ s}^{-1}$. This is lower than the literature value for the diffusion constant of $2.94 \times 10^{-5} \text{ cm}^2 \text{ s}^{-1}$ of deuterated water found at a temperature of 318 K [63]. The reduced diffusion constant observed in our study is attributed to a restricted mobility of the water molecules bound to the hydration shell of the polymer micelles.

Figure 8 reproduces the linewidth taken at IN3 (ILL) with the shear device for Q values between 0.3 and 1.7 \AA^{-1} and for a temperature of 313 K. Only one orientation of the shear device with Q either perpendicular or parallel to the flow provides useful information. For this reason triple-axis spectroscopy is better suited for this kind of experiments than time of flight. The left panel displays data taken with the sample in reflection geometry and the right panel data taken with the sample in transmission geometry at rest and with an applied shear rate of 6000 s^{-1} . The quasielastic linewidths are plotted versus Q^2 . In addition the Q^2 fit to the NEAT data is shown for comparison as solid line. Due to the shadow of the shear device in reflection geometry, only a restricted Q range was accessible. All data show for higher Q values the same Q dependence as found in the time-of-flight experiment. The reason for the discrepancy of the time-of-flight and triple-axis data results from the worse resolution for the triple-axis measurements. The data reveal that the diffusion of the water molecules in the sample is not affected by the applied shear and stays isotropic in the two directions that have been addressed. The inelastic Doppler-scattered intensity from the flowing liquid is not visible in this experiment. The expected energy transfer is of the order of 30 \mu eV and thus much smaller than the instrumental resolution.

2. Polymer

The dynamics in the μeV energy range have been investigated using the neutron backscattering spectrometer IN16

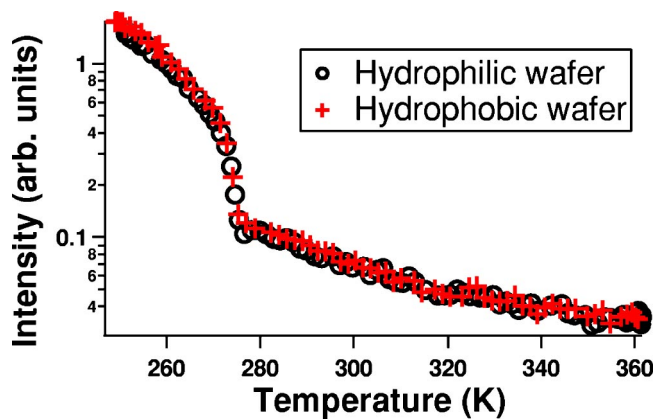


FIG. 9. Elastic scattering of a sample of a 33% (in weight) solution of P85 in deuterated water plotted over the temperature for $Q=1.4 \text{ \AA}^{-1}$.

(ILL). For these measurements hydrophilic and hydrophobic-coated silicon wafers have been mounted as wall material in the shear device. The aluminum and stainless steel interfaces used in the triple-axis and rheological studies show a hydrophilic property.

To investigate the diffusion of the sample at rest, we prepared two samples in a flat geometry container (rectangular gap of 0.6 mm with 30- and 50-mm edges) with hydrophilic/hydrophobic silicon interfaces in a cryostat. Figure 9 shows the elastically scattered intensity at $Q=1.4 \text{ \AA}^{-1}$ as a function of temperature between 250 and 360 K. The drop in the detected intensity at 273 K is a signature of the melting of the deuterated water acting as solvent.

Figure 10 shows a zoom into the flat decreasing region between temperatures of 275 and 360 K overlaid with the phase diagram obtained from rheology. In this representation one can distinguish different slopes that can be related to the different phases. It is visible that the intensity is not increased for the more viscous phases as would be expected from the Stokes-Einstein-Debye model even if the diffusivity is affected by the phase transitions. The two different interfaces have no influence on this phase transition. This is in good agreement with the diffraction study where only minor differences in the structure were found for the static sample.

Figure 11 shows the Q dependence of the linewidth of the Lorentzian line fitted to the data and plotted versus Q^2 . Again

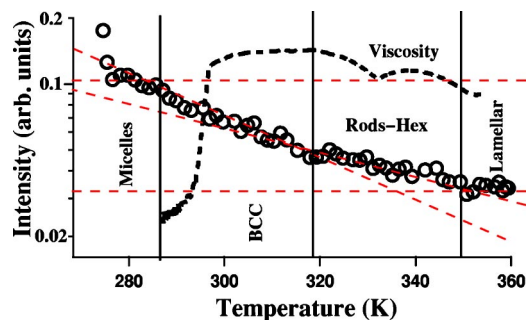


FIG. 10. Flat decreasing region of the elastic scattering of a sample of a 33% (in weight) solution of P85 in deuterated water plotted over the temperature for $Q=1.4 \text{ \AA}^{-1}$.

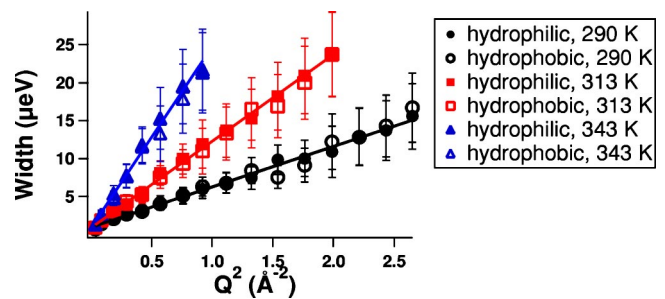


FIG. 11. Linewidth for the narrow quasielastic line.

a Q^2 dependence is found, from which we infer a translational jump diffusion however 10 times slower than for the solvent. The intensity exhibits a more or less equal distribution for the different Q values as expected for a dominantly incoherent scatterer like the polymer monomers. From the slope of the linewidth versus Q^2 the diffusion constant can be calculated and is listed in Table III for the different temperatures. For a 10% solution of similar pluronics P104, P123, and F128 a diffusion constant of $2 \times 10^{-7} \text{ cm}^2 \text{ s}^{-1}$ has been found from light scattering at a temperature of 298 K for the monomer [49]. The slightly higher diffusion constant deduced from our investigations may be correlated to the higher polymer concentration or the different monomer molecules.

Figure 12 shows quasielastic spectra taken with a 0.6-mm-thick sample (10% scattering) in the shear device at a temperature of 291 K and for $Q=1.4 \text{ \AA}^{-1}$. At this Q value the quasielastic linewidth, found in the static measurement, is well visible and analyzable. In addition optimizing the energy resolution enforces retaining the backscattering condition at the analyzer and thus a compact mounting of the shear device and the detector in reflection as well as in transmission geometry. These geometrical restrictions are best fulfilled for a scattering angle of 90° , meaning $Q=1.4 \text{ \AA}^{-1}$. Nevertheless, the instrumental resolution determined to be $1.4 \mu\text{eV}$ was slightly reduced with respect to the optimal value of less than $1 \mu\text{eV}$. For the measurements under shear the velocity of the moving surface was 1.3 m/s. The left panels show data taken with the hydrophilic interface as wall material of the moving and fixed disks and the right panels show data taken with the hydrophobic interface. The two upper panels correspond to data taken with the sample at rest. The elastic line for the upper panels in reflection geometry (first line) as well as in transmission geometry (second line) is quasielastically broadened. All spectra have been fitted by a Gaussian and a Lorentzian line. First the elastic line of the empty cell was determined and then used as a fixed parameter. The two spectra on the left side show a similar line width of $2\Gamma=11.5 \pm 1 \mu\text{eV}$ (FWHM) and $2\Gamma=11.6 \pm 1 \mu\text{eV}$. From Fick's law $D=\Gamma/(\hbar Q^2)$ the diffusion

TABLE III. Diffusion constants for the polymer monomers for different temperatures.

T [K]	290	313	343
D [$10^{-6} \text{ cm}^2/\text{s}$]	0.4 ± 0.05	0.9 ± 0.1	1.8 ± 0.2

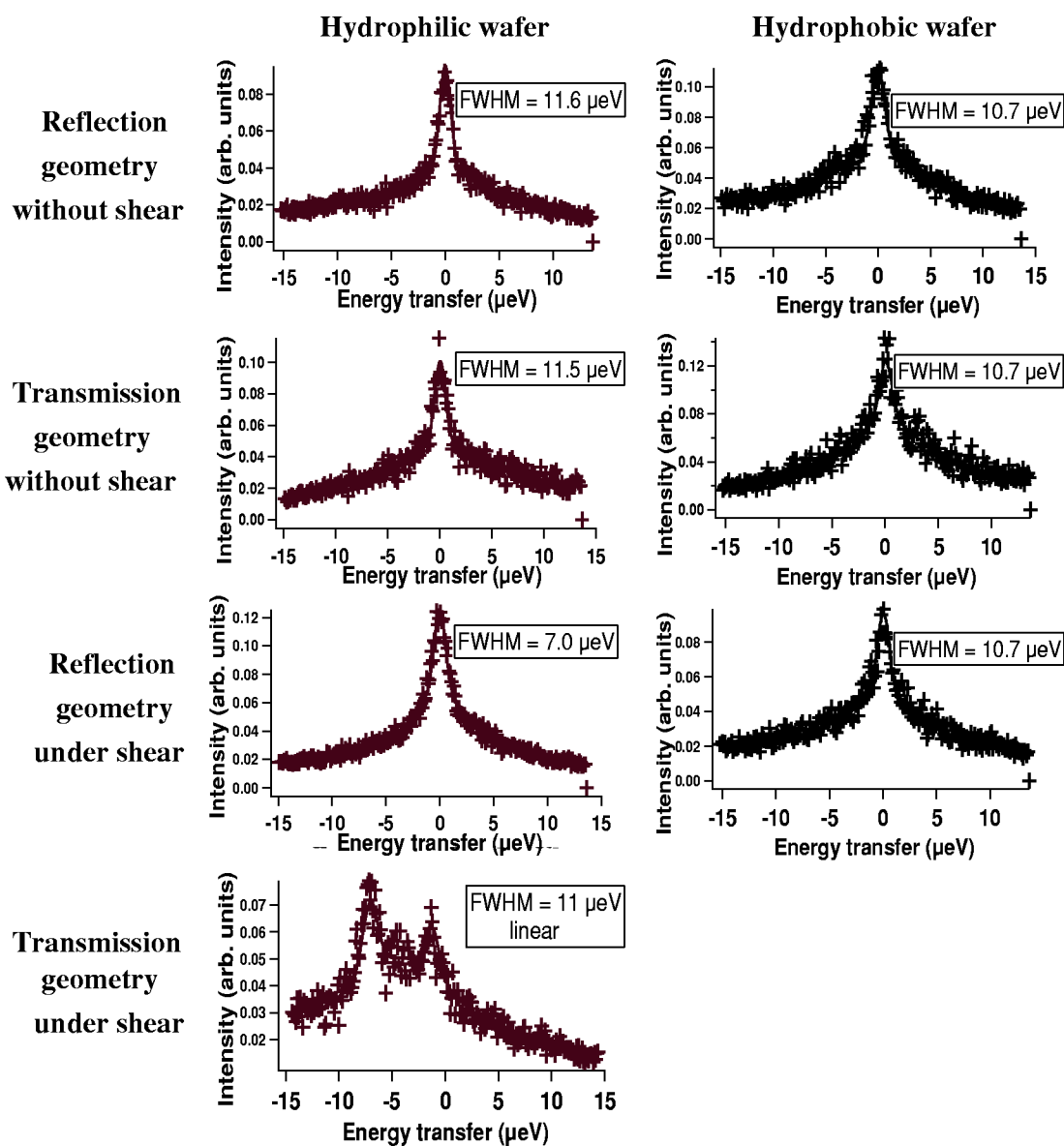


FIG. 12. Quasielastic spectra taken with a sample of a 33% (in weight) solution of P85 in deuterated water at a hydrophilic (left panels) and a hydrophobic interface (right panels). The top panels show data taken with the sample at rest either in reflection or in transmission geometry and the bottom panels show data taken at a shear rate of 2200 s^{-1} .

constant is $D=4.4\pm 0.5\times 10^{-7} \text{ cm}^2 \text{ s}^{-1}$. For the sample in contact with the hydrophilic interface the line narrows under shear (2200 s^{-1}) to $7.0\pm 0.7 \mu\text{eV}$ ($D=2.7\pm 0.4\times 10^{-7} \text{ cm}^2 \text{ s}^{-1}$) in reflection geometry but remains unchanged $11\pm 1 \mu\text{eV}$ ($D=4.2\pm 0.3\times 10^{-7} \text{ cm}^2 \text{ s}^{-1}$) in transmission geometry. This shows that under shear the diffusion constant becomes reduced in the direction of the shear gradient and changes from being isotropic without shear to anisotropy under shear on a length scale of 4.5 \AA , with the diffusion coefficient in the direction of the shear gradient being smaller than that in the direction of the flow.

To fit the data in transmission geometry under shear we calculated the scattering law including the inelastic part from Doppler-scattered neutrons. Due to the large quasielastic linewidth and the statistics, a fit of the inelastic Doppler-scattered part of the spectrum and therefore the macroscopic

velocity profile was not possible [64]. A fit with a linear velocity profile was assumed; different profiles will not change appreciably the fit to the linewidth.

For the hydrophobic interface shear has no influence on the quasi elastic linewidth in reflection geometry. All data are well described with a linewidth of $10.7\pm 1 \mu\text{eV}$ and are within the error bars similar to that obtained from the data taken for the hydrophilic interface.

V. DISCUSSION

In the following sections the results obtained by the different experimental methods will be discussed and brought into context.

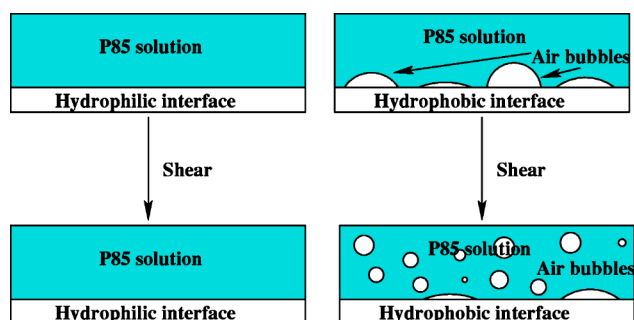


FIG. 13. Effect of air bubbles formed at the solid-liquid interface for the formation of structure in liquids under shear.

A. Properties of the micelles: Microscopic structure

As seen in Fig. 5 the reflectivity measured for the sample in contact with a hydrophobic interface drops faster than that found for the sample in contact with a hydrophilic interface. From this we infer an increased interfacial roughness at the hydrophobic interface. The reason for this is twofold.

First, as the polymer micelles as well as the water tries to avoid coming close to the interface air bubbles may be formed close to the solid interface. Figure 13 elucidates this effect. By applying shear the interface region becomes disturbed and the bubbles may move away from the interface. This implies an increase in defect density in the bulk medium and with increasing shear the bubbles tend to destroy the crystalline structure. On the other hand most of the applied stress will be relaxed in the air bubbles as their modulus is much lower than that of the solution. This results in a reduced stress on the sample.

Second, the polymer micelles, with their hydrophilic shell, cannot arrange themselves close to the hydrophobic interface because of the electrostatic repulsion. As clearly seen from the reflectivity data, no surface micelles are formed. Surface micelles should show up as thickness oscillations in the reflectivity, as their size would be on the order of 100 Å. Figure 14 elucidates the effect of defects formed at the solid-liquid interface. As discussed for the air bubbles

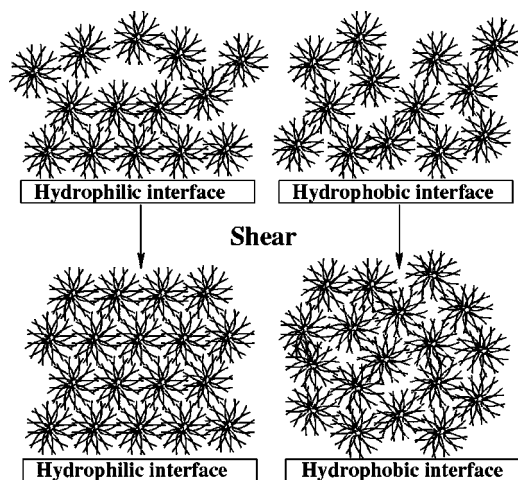


FIG. 14. Effect of defects formed close to the solid-liquid interface for the formation of structure in liquids under shear.

with the sample at rest, first defects are formed close to the solid-liquid interface. On the other hand, for the hydrophilic interface the first layers of micelles form a crystalline structure. The structure of Pluronic F127 micelles close to a hydrophilic and a hydrophobic interface has recently been explored in more detail [59] supporting the above statement. As the sample becomes sheared the crystalline planes rearrange themselves for the hydrophilic interface and the crystalline structure stretches throughout the whole sample. In contrast, at the hydrophobic interface there are no crystalline planes to arrange and the number of defects increases with increasing shear in the bulk sample. At this time defects formed at the interface get dissolved and disturb the structure in the bulk.

Both of the effects discussed above superimpose and enhance each other.

B. Viscosity: Microscopic dynamics

The phase transitions found in the measurements of the viscosity seem to have influence on the microscopic diffusion investigated. According to the Stokes-Einstein-Debye model [Eq. (6)] the diffusion constant should change proportional to the changes of the viscosity and the particle radius. It is known that the size of the micelles increases continuously with temperature. For the present experimental parameters we can assume less than a doubling of the radius which is negligible in comparison to the jumps in the viscosity at the phase transitions. The increase in viscosity implies a decrease of the diffusion constant by several orders of magnitude for the cubic phase with respect to the micelle phase.

As there are only short-range micelle-micelle correlations in the liquid phase the diffusion constant of the micelles can be calculated directly from the Stokes-Einstein-Debye model. For a micelle radius of 60 Å one finds a diffusion constant of $3.6 \times 10^{-9} \text{ cm}^2 \text{ s}^{-1}$. With the technique of neutron backscattering, diffusion constants of about $10^{-7} \text{ cm}^2 \text{ s}^{-1}$ are accessible. The translational mode found in this work is on the order of $10^{-6} \text{ cm}^2 \text{ s}^{-1}$ and for the time-of-flight and triple-axis experiment $10^{-5} \text{ cm}^2 \text{ s}^{-1}$. The length scale on which the diffusion constants were probed is on the order of 2–10 Å. This means that the observed diffusive processes occur in and between the micelles. Nevertheless, from the elastic scan, Fig. 10, it can be seen that the observed local particle diffusion is affected by the different arrangements of the micelles but cannot be described by the Stokes-Einstein-Debye model. This demonstrates that the monomer motion is to some extent coupled to the structure formed by the micelles and correlates well with our observations made for the sheared sample, when an effect of shear on the local dynamics was found for strong structural correlations. The explanation for this effect is that the micelles are strongly interconnected and the sample is in a percolated state.

C. Macroscopic flow: Microscopic dynamics

Calculations predict that the self-diffusion tensor on both the short- and long-time scales becomes anisotropic for shear rates greater than 10^{10} s^{-1} [26,27,65]. It was found that the diffusion constant in the direction of the flow becomes increased for about 10%, whereas it becomes decreased in the

TABLE IV. Experimental parameters.

Particles	η [Pas]	r_h [\AA]	m [u]	$\dot{\gamma}$ [s^{-1}]	D [cm^2/s]
D ₂ O molecule	0.1	3	20	2200	4×10^{-6}
P85 monomer	0.1	15	4522	2200	5×10^{-7}
P85 micelle	0.1	60	226000	2200	3.5×10^{-9}
Particles	τ_B [s]	τ_I [s]	Re	Pe	
D ₂ O molecule	5.9×10^{-17}	3×10^{-10}	8×10^{-4}	6.6×10^{-7}	
P85 monomer	2.7×10^{-16}	4.5×10^{-8}	8×10^{-4}	1×10^{-4}	
P85 micelle	3.3×10^{-15}	1×10^{-4}	8×10^{-4}	0.22	

two other directions for about 20%. To further confirm this effect higher shear rates are desirable. However, they are experimentally hardly achievable.

Experimentally a different behavior was found for a colloidal system. On the time scale of seconds the diffusion of particles with a diameter of about 100 μm has been investigated [34]. For a Peclet number $\text{Pe} \sim 1$ an anisotropic diffusion is induced from the shear field. The authors show that the component in the direction of the shear gradient is increased with respect to that perpendicular to the flow. In addition, the shear-induced diffusion heavily depends on the concentration of the particles in the solution and a maximum of the effect was found for a concentration of about 50% in volume. For similar systems additional nonequilibrium molecular-dynamic simulations have been performed and, qualitatively, the same behavior was found as in the experiment over a large range of Peclet numbers (10^{-2} – 10^4) and for concentrations up to 60% [65].

The micelle concentration in our sample is close to 50% in volume as we are working close to the critical micelle concentration for crystallization. As the micelles can be described as “core and gown” particles consisting out of monomers our sample should show properties similar to a colloidal as well as to a molecular system.

In Table IV the Peclet number, Reynolds number, and other important experimental parameters are summarized for the present measurements. The Reynolds numbers are small and no turbulence should develop.

The motion on the short-time scale is in the fs regime and too fast for neutron scattering. The second process that has to be considered is the diffusion on the long-time scale and to evaluate the importance of shear to the diffusion the Peclet number. For the water molecules this number is about 10^{-7} and shear does not affect the microscopic diffusion as found in the triple-axis experiment. The Peclet number for the micelles is about 0.2, and therefore one would expect an effect of shear on the diffusion. On the other hand, the relaxation time of the micelles is in the μs -to- ms regime and therefore too slow for neutron backscattering. The Peclet number of the monomer is about 10^{-4} and thus too small to expect a direct influence of shear on the diffusion. Nevertheless, for the calculations spherical particles have been assumed. The monomers are highly stretched in the micelles, and the assumption of spherical particles might not be correct. For a stretched chain the different lengths of the different axes has

to be considered and for the long axis 4 times bigger than the radius one will obtain a Peclet number increased by a factor of about 65. In addition, the monomers are highly entangled and thus cannot be treated as independent particles interacting via a simple potential, as assumed in the model. This statement is confirmed by our backscattering data that show that the monomer diffusion is coupled to the structural arrangements of the polymer micelles. Considering this, an impact of shear on the microscopic local diffusion of the monomers may be expected. Due to the shear gradient, the local environment of the monomers, for the highly structured sample, becomes anisotropic even if the monomers are inside the micelles. From the pronounced Bragg reflection found in the diffraction data it is clear that while building up a highly ordered structure the sample becomes more and more phase separated and the difference in the scattering length density becomes increased. Because of this phase separation, the monomer concentration in the micelles increases. This means a decrease in the mobility of the single monomers and therefore a smaller diffusion constant along the direction of the shear gradient. The reduction found in the present experiment is 63% and thus bigger than expected for a simple molecular system. Because of the short length scale, which was investigated, no influence of shear on the diffusivity as expected for a colloidal system was found. For the hydrophobic interface most of the shear is taken up by the defects and therefore no effect of shear on the diffusivity of the monomers was found.

VI. CONCLUSION

In summary we have characterized the microscopic diffusion in a polymer solution under shear over several orders of magnitude in time on the molecular length scale. The diffusivity of the solvent molecules as well as that of the polymer monomers has been addressed. By the use of different chemical terminations at the solid-liquid interface we were able to induce different degrees of structural order to the sample under shear. The results of our measurements are summed up in the following points.

(i) We find the local monomer dynamics due to the percolated state of the sample coupled to the structural arrangements of the micelles.

(ii) For strong micelle-micelle correlations we find the diffusivity to become reduced in the direction of the shear gradient but unchanged in the direction of the flow meaning an anisotropy under shear.

(iii) For weak correlations we find no influence of shear on the diffusivity.

(iv) We find the structural arrangements of the micelles under shear to depend on the chemical termination of the solid-liquid interface.

ACKNOWLEDGMENTS

We acknowledge financial support of the DFG (Grant Nos. MA801/17 and ZA161/4) and the BMBF (Grant No. ADAM 04ZAE8BO). We also acknowledge the help of F. Demmel during the experiment on IN3, that of J. Pieper, R. Lechner, and A. Desmedt during the experiment on NEAT, and that of V. Leiner and R. Siebrecht during the experiment on ADAM.

-
- [1] A. Keller, E. Pedemonte, and F. M. Willmouth, *Nature (London)* **225**, 538 (1970).
- [2] J. B. Hayter and J. Penfold, *J. Phys. Chem.* **88**, 4589 (1984).
- [3] Ch. Thurn, J. Kalus, and H. Hoffmann, *J. Chem. Phys.* **80**, 3440 (1984).
- [4] K. A. Koppi *et al.*, *J. Phys. II* **2**, 1941 (1992).
- [5] P. Lindner and Th. Zemb, *Steady-State SANS Experiments under External Constraints*, edited by (Elsevier, Amsterdam, 1991).
- [6] O. Diat, D. Roux, and F. Nallet, *J. Phys. II* **3**, 1427 (1993).
- [7] D. Roux, F. Nallet, and O. Diat, *Europhys. Lett.* **24**, 53 (1993).
- [8] O. Diat and D. Roux, *J. Phys. II* **3**, 9 (1993).
- [9] V. S. J. Craig, C. Neto, and D. R. M. Williams, *Phys. Rev. Lett.* **87**, 054504 (2001).
- [10] Y. Zhu and S. Granick, *Phys. Rev. Lett.* **87**, 096105 (2001).
- [11] W. B. Black and M. D. Graham, *Macromolecules* **34**, 5731 (2001).
- [12] M. Cieplak, J. Koplik, and J. R. Banavar, *Phys. Rev. Lett.* **86**, 803 (2001).
- [13] R. Makhlofi *et al.*, *Europhys. Lett.* **32**, 253 (1995).
- [14] R. W. Mair and P. T. Callaghan, *Europhys. Lett.* **36**, 719 (1996).
- [15] E. Fischer and P. T. Callaghan, *Phys. Rev. E* **64**, 011501 (2001).
- [16] M. M. Britton and P. T. Callaghan, *Eur. Phys. J. B* **7**, 237 (1999).
- [17] M. M. Britton and P. T. Callaghan, *Phys. Rev. Lett.* **78**, 4930 (1997).
- [18] J.-F. Berret, G. Porte, and J.-P. Decruppe, *Phys. Rev. E* **55**, 1668 (1997).
- [19] L. Sandrin, S. Manneville, and M. Fink, *Appl. Phys. Lett.* **78**, 1155 (2001).
- [20] J.-B. Salmon *et al.*, *Phys. Rev. Lett.* **90**, 228303 (2003).
- [21] J.-B. Salmon *et al.*, *Eur. Phys. J. E* **10**, 209 (2003).
- [22] M. Wolff *et al.*, *Mater. Sci. Eng., B* **34**(6), 568 (2003).
- [23] S. Sarman, D. J. Evans, and P. T. Cummings, *Phys. Rep.* **305**, 1 (1998).
- [24] J. W. Dufty, *Phys. Rev. A* **30**, 1465 (1984).
- [25] S. Sarman, P. J. Daivis, and D. J. Evans, *Phys. Rev. E* **47**, 1784 (1993).
- [26] C. Marin and V. Garzo, *Phys. Rev. E* **57**, 507 (1998).
- [27] S. Sarman, D. J. Evans, and A. Baranyai, *Phys. Rev. A* **46**, 893 (1992).
- [28] D. L. Malandro and D. J. Lacks, *Phys. Rev. Lett.* **81**, 5576 (1998).
- [29] P. T. Cummings *et al.*, *J. Chem. Phys.* **94**, 2149 (1991).
- [30] D. M. Heyes *et al.*, *J. Chem. Phys.* **73**, 3987 (1980).
- [31] J. D. Moore *et al.*, *J. Non-Newtonian Fluid Mech.* **93**, 83 (2000).
- [32] X. Qiu *et al.*, *Phys. Rev. Lett.* **61**, 2554 (1988).
- [33] D. Rusu *et al.*, *Polymer* **40**, 1353 (1999).
- [34] V. Breedveld *et al.*, *Phys. Rev. E* **63**, 021403 (2001).
- [35] W. Xue and G. S. Grest, *Phys. Rev. A* **40**, 1709 (1989).
- [36] L. Van Hove, *Phys. Rev.* **95**, 249 (1954).
- [37] M. Bee, *Quasielastic Neutron Scattering*, 1st ed. (Hilger, Bristol, 1988).
- [38] L. D. Landau and E. M. Lifschitz, *Lehrbuch der theoretischen Physik* (Akademie-Verlag, Berlin, 1966).
- [39] A. Einstein, *Ann. Phys. (Leipzig)* **17**, 549 (1905).
- [40] K. Mortensen, *J. Phys.: Condens. Matter* **8**, A103 (1996).
- [41] K. Mortensen and Y. Talmin, *Macromolecules* **28**, 8829 (1995).
- [42] K. Mortensen, *Macromolecules* **30**, 503 (1997).
- [43] K. Mortensen, W. Brown, and B. Norden, *Phys. Rev. Lett.* **68**, 2340 (1992).
- [44] I. Goldmints *et al.*, *Langmuir* **15**, 1651 (1999).
- [45] L. Fabbian *et al.*, *Phys. Rev. E* **59**, R1347 (1999).
- [46] J. Bergholtz and M. Fuchs, *Phys. Rev. E* **59**, 5706 (1999).
- [47] L. Lobry *et al.*, *Phys. Rev. E* **60**, 7076 (1999).
- [48] W.-R. Chen, S.-H. Chen, and F. Mallamace, *Phys. Rev. E* **66**, 021403 (2002).
- [49] G. Wanka, H. Hoffmann, and W. Ulbricht, *Colloid Polym. Sci.* **268**, 101 (1990).
- [50] R. Siebrecht, Ph.D. thesis, Ruhr-Universitt-Bochum, 2000.
- [51] K. Lum, D. Chandler, and J. D. Weeks, *J. Phys. Chem.* **103**, 4507 (1999).
- [52] A. J. Pertsin, T. Hayashi, and M. Grunze, *J. Phys. Chem. B* **106**, 12 274 (2002).
- [53] J. W. G. Tyrrell and P. Attard, *Phys. Rev. Lett.* **87**, 176104 (2001).
- [54] D. Schwendel *et al.*, *Langmuir* **19**, 2284 (2003).
- [55] R. Steitz *et al.*, *Langmuir* **19**, 2409 (2003).
- [56] K. Mortensen, D. Schwahn, and S. Janssen, *Phys. Rev. Lett.* **71**, 1728 (1993).
- [57] B. Frick, *et al.*, *Chem. Phys.* **292**, 311 (2003).
- [58] M. Wolff *et al.*, *Appl. Phys. A: Mater. Sci. Process.* **374**, A74 (2002).
- [59] M. Wolff *et al.*, *Phys. Rev. Lett.* **92**, 255501 (2004).

- [60] A. R. Wildes, J. Mayer, and K. Theis-Bröhl, *Thin Solid Films* **401**, 7 (2001).
- [61] J. A. Polo and P. A. Egelstaff, *Phys. Rev. A* **27**, 1508 (1983).
- [62] F. Hajdu, S. Lengyel, and G. Palinkas, *J. Appl. Crystallogr.* **9**, 134 (1976).
- [63] R. Mills, *J. Phys. Chem.* **77**, 685 (1973).
- [64] M. Wolff *et al.*, *J. Phys.: Condens. Matter* **15**, S337 (2003).
- [65] D. R. Foss and J. F. Brady, *J. Fluid Mech.* **401**, 243 (1999).